IEEE Access
Multidisciplinary | Rapid Review | Open Access Journal

Received April 21, 2021, accepted May 4, 2021, date of publication May 7, 2021, date of current version May 17, 2021.

Digital Object Identifier 10.1109/ACCESS.2021.3078315

Estimation of Islanding Events in Utility Distribution Grid With Renewable Energy Using Current Variations and Stockwell Transform

OM PRAKASH MAHELA[1], (Senior Member, IEEE), YAGYA SHARMA[2], SHOYAB ALI[2], BASEEM KHAN[3], (Member, IEEE), AND SANJEEVIKUMAR PADMANABAN[4], (Senior Member, IEEE)

[1]Power System Planning Division, Rajasthan Rajya Vidyut Prasaran Nigam Ltd., Vidyut Bhawan, Jaipur 302005, India
[2]Department of Electrical Engineering, Vedant College of Engineering and Technology, Bundi 323021, India
[3]Department of Electrical and Computer Engineering, Hawassa University, Hawassa 1530, Ethiopia
[4]CTiF Global Capsule, Department of Business Development and Technology, Aarhus University, 7400 Herning, Denmark

Corresponding author: Baseem Khan (baseem.khan04@gmail.com)

ABSTRACT This research work has designed an algorithm to identify islanding events using the current signals in a distribution grid interfaced with renewable energy (RE) sources situated in remote areas. A median-based islanding recognition factor (MIRF) is designed by processing the current signal using Stockwell transform (ST). A current rate of change of islanding recognition factor (CRCIRF) is computed by differentiating the root mean square (RMS) current concerning time. The MIRF and CRCIRF are multiplied element by element to calculate the current-based islanding recognition factor (IRFC) used to recognize islanding events and non-islanding events. Simple decision rules are used to discriminate Islanding events from the faulty and the operational events by comparing peak magnitude of IRFC with pre-set threshold values. This IDM effectively recognizes islanding events in the presence of noise with 10 dB signal-to-noise ratio (SNR) level. The performance of IDM is established on a practical distribution feeder. Developed work is executed in MATLAB/Simulink.

INDEX TERMS Distribution grid, islanding event, renewable energy, Stockwell transform.

NOMENCLATURE

ABPNN	Adaptive back propagation neural network
AI	Artificial intelligence
BRPV	Bilateral reactive power variation
CB	Circuit breaker
CRCIRF	Current rate of change of islanding recognition factor
CWT	Continuous wavelet transform
DFIG	Doubly fed induction generator
DG	Distributed generation
DLA	Deep learning architecture
DWT	Discrete Wavelet transform
EkNN	Ensemble k-nearest neighbour
EMD	Empirical mode decomposition
FFT	Fast Fourier transform
GCPVSs	Grid-integrated photovoltaic systems
ICT	Interconnecting transformer
IDM	Islanding detection method
IDS	Islanding detection scheme
IEEE	Institute of electrical and electronics engineers
IMF	Intrinsic mode functions
IRFC	Islanding recognition factor
IRL	Islanding relay
ISC	Informative sparse representation-based classification
IR	Root-mean-square values of the current
IRFC	Islanding recognition factor
LEE	Log energy entropy
LG	Line to ground fault
LL	Two-phase fault
LLG	Two-phase to ground fault
LLLG	Three-phase to ground fault
MGP	Multi-gene genetic programming
MFO	Moth flame optimization
MIRF	Median based islanding recognition factor
ML	Machine learning
MM	Mathematical morphology

The associate editor coordinating the review of this manuscript and approving it for publication was Amjad Anvari-Moghaddam.

MPP	Maximum power point
MPPT	Maximum power point tracking
NSC	Negative sequence component
NDZ	Non-detection zone
OV	Over-voltage
PCC	Point of common coupling
PIP	Pseudo islanding phenomenon
PV	Photovoltaic
RE	Renewable energy
RF	Random forest
RFMFO	Random forest moth flame optimization
RMS	Root mean square
ROCOC	Rate of change of current
ROCOF	Rate of change of frequency
ROCOV	Rate of change of voltage
RPNN	Ridgelet probabilistic neural network
RPV	Reactive power variation
SLT	Slantlet Transform
SNR	Signal to noise ratio
SPP	Solar power plant
SRFT	Synchronous reference frame transformation
SSE	Singular spectrum entropy
ST	Stockwell transform
STFT	Short-time Fourier transform
SVM	Support vector machine
THD	Total harmonic distortion
TMC	Threshold magnitude
TVF	Time-varying filter
UV	Under voltage
VCI	Voltage controlled inverter
VU	Voltage unbalance
WFC	Current based weight factor
WG	Wind generator
WPP	Wind power plant
WT	Wavelet transform

I. INTRODUCTION

The distribution network in India is changing from passive nature to dynamic nature at a fast rate due to the integration of the distributed generation (DG) plants. In this network, DG sources continue to supply loads when the utility grid is disconnected; this scenario is known as the island mode of operation. The process of disconnection of the distribution network from the utility grid is known as islanding. This event should be identified quickly, and DG must be disconnected from the distribution network [1]. This will help to provide safety to personnel involved in the operation and maintenance of the utility grid and generators. This will also avoid damages to the equipment due to varying frequency and voltage in the islanded scenario. As per standard IEEE 1547 and UL 1741, the DG should be disconnected from the grid within 2s after the islanding event incidence. Islanding detection methods (IDM) are classified as remote and local IDMs. Remote IDMs use a communication channel between the utility grid and DG. Local IDMs take decisions based on information collected by measurements performed at the DG location. These methods are passive and active. Passive IDMs are based on evaluating the system parameters like voltage and frequency at the point of standard coupling (PCC) to detect islanding events. These methods suffer from the problem of a long time for operation in a balanced or small power mismatch scenario resulting in a sizeable non-detection zone (NDZ) [2]–[5]. This problem can be eliminated using signal processing techniques that effectively track even the small magnitude changes in the system parameters.

A. RELATED WORK

A critical review of the techniques about the islanding detection approaches is discussed and detailed in this section. Research using signal processing techniques, machine learning approaches, deep learning approaches, and traditional methods about islanding identification is discussed in this section. Samui and Samantaray [6] designed an analytical approach-based IDM for the DG integrated into the grid using a constant voltage-controlled inverter (VCI). This IDM effectively detects the islanding by controlling the inverter output. This approach effectively eliminates the reliance of DG operation point on the performance of the anti-islanding design. However, the effect of noise on the performance of IDM has not been investigated in this study. In [7], a deep learning supported technique is designed to detect and differentiate islanding events from grid disturbances. The features to recognize island events and grid disturbances are computed using a hybrid combination of wavelet transform (WT), multi-resolution singular spectrum entropy (SSE), and deep learning architecture (DLA). This IDM has low accuracy of 94%, and performance is affected when the noise level is high. Multi-gene genetic programming (MGP) based IDM to detect islanding events of DG sources is reported in [8]. This method has a high degree of dependability for accurately discriminating the islanding scenario from the operational events and other grid disturbances, including load switching, disconnection of DG, grid integration of DG, and faulty phenomenon. This method is a computational intelligence approach and effectively detects the DG islanding with high accuracy. A hybrid mechanism using a combination of random forest (RF) and moth flame optimization (MFO) designated as RFMFO for islanding recognition in a DG source-based distribution grid is investigated in [9]. It has the merit of minimum NDZ and maintains good quality of power. In [10], the authors introduced a method that uses the sensitivity of 6 different parameters of a power system to identify the islanding event. This technique effectively discriminates the islanding event to a small power mismatch of 0.14 MW and 0.11 MVAR, indicating improved accuracy and minimum effect on power quality. This has a demerit of high islanding detection time of 2s. Thomas *et al.* [11] suggested an IDM that uses the features computed from reactive power using empirical mode decomposition (EMD). This technique has very low NDZ without affecting the quality of power. However, this IDM identifies the islanding event in

a time duration of two cycles. In [12], the authors proposed a hybrid IDM that combines the passive IDM of voltage unbalance and total harmonic distortion (VU/THD) with an active approach based on bilateral reactive power variation (BRPV). This effectively identifies the islanding event in the presence of inverter-based DG units with improved performance. In [13], the authors proposed an IDM that can be implemented to recognize islanding events in a grid with multiple DG units. A voltage index is introduced, which effectively detects islanding operation even during the scenario of large power mismatches with zero NDZ. It has a high detection time of 0.3s. An IDM for identifying islanding scenarios using quadratic time-frequency decomposition using the HSS-Transform of 3-phase signals computed using the synchronous reference frame transformation (SRFT) is investigated in [14]. Informative sparse representation-based classification (ISC) is used for developing comprehensive artificial intelligence (AI) architecture to discriminate the islanding events from the non-islanding disturbances incident on the grid. This ISC technique does not require any training method and uses a linear mathematical formulation. This approach is fast and has a minimum computational burden. In [15], a method is investigated for detecting islanding events in the presence of grid-integrated photovoltaic systems (GCPVSs). This method used the disturbance injection at the time of maximum power point tracking (MPPT). Absolute output voltage deviation is used to apply the disturbance to move the system's operating point from its maximum power point (MPP). It is efficient for micro-grid applications using power injection at the maximum point for catering to critical loads and maintains system stability. An islanding detection scheme (IDS) for DG source-based distribution network that effectively minimizes NDZ using a pattern-recognition approach is introduced in [16]. A hybrid combination of time-frequency signal decomposition and machine learning (ML) techniques is used to process the voltage signal to identify an islanding scenario. Intrinsic mode functions (IMF) are introduced to increase the time-frequency resolution of the non-stationary signal and a random subspace ensemble architecture using ensemble k-nearest neighbor (EkNN) classifier. It is implemented for identifying islanding events by application of feature vector computed using IMF. It requires reliability analysis due to which computational complexity increases. In [17], and IDM has introduced a grid integrated solar photovoltaic (PV) inverter by applying multi-signals. It is based on the use of Slantlet Transform (SLT), log energy entropy (LEE), and an advanced ML assisted Ridgelet Probabilistic Neural Network (RPNN). This IDM has high accuracy but suffers from a high computational burden. An IDM driven by a combination of adaptive backpropagation neural network (ABPNN) and support vector machine (SVM) considering pseudo islanding phenomenon (PIP) using frequency and reactive power variation (RPV) is investigated in [18]. This is more effective compared to the conventional active IDMs. This is a relatively slow method and not effective during faulty events. In [19], a passive IDM to detect islanding using an advanced signal decomposition approach based on the time-varying filter-based empirical mode decomposition (TVF-EMD) is investigated. Thus, the method uses computational energy to assess the islanding case. It is effective even in the presence of non-linear loading conditions. Kaushik *et al.* [20] introduced an IDM for identifying events such as islanding, grid integration, and outage of solar PV and wind generator (WG) plants in the grid by applying ST. Islanding events might be incidents with different nature of power injection in the grid. The algorithm is implemented to recognize the events by processing negative sequence components (NSC) of voltage using ST. Various features computed from the ST output are used to identify the events and transient scenarios. Recognition of the different RE sources at the instant of integration is also achieved using the algorithm. The algorithm is also tested for the noisy scenarios considering 10dB SNR. This IDM is better due to small NDZ, low computation time, and less influenced by noise than time-frequency transform coefficients of the voltage signal. There are various techniques for optimal placement of DGs in the utility grid, optimal sizing of DGs, application of battery energy storage, off-grid applications of DGs, optimal solar PV system design, wind energy system & hybrid energy systems are investigated by authors in [21]–[25]. These studies will help to design the remotely located distribution grids for the different scenarios to implement the IDMs.

B. RESEARCH GAPS

A detailed analysis of the techniques reported in the literature and discussed in the above section is carried out. It is pointed out that the signal processing methods are gaining momentum in identifying the islanding events. However, present passive IDMs use under/over frequency, under/over voltage, current harmonics, voltage phase jump, and voltage harmonics to recognize Islanding events. Passive methods suffer from the disadvantages of significant detection time and large NDZ. It can be mitigated by combining the system parameter variations with the features computed using the various signal processing techniques. It will help to minimize the islanding detection time and to achieve improved efficiency. It is considered a vital concept for the research and included designing a hybrid IDM algorithm for renewable energy-based power grids.

C. CONTRIBUTION OF THE WORK

The research included in this paper aims to identify the islanding event in a distribution network to which RE sources are integrated. The main contributions of the paper are detailed below:-

- A passive IDM is designed based on the hybrid combination of non-signal processing and signal processing approaches of passive IDMs.
- Rate of RMS current (ROCOC) change and median-based feature computed by processing the current signals using Stockwell transform are used to design the islanding

recognition factor (IRFC) to identify the islanding events in remotely located distribution grid with the availability of RE.
- Islanding events are differentiated from the faulty events and operational events using decision rules by comparing the peak magnitude of IRFC with pre-set threshold values (TMC1 and TMC2).
- The proposed algorithm effectively detects the islanding events in the availability of wind energy and solar energy. This IDM also effectively discriminates the islanding events from faulty and operational possibilities.
- This IDM effectively recognizes islanding events in the presence of noise with a high noise level of 10 dB SNR.
- Proposed IDM is tested to implement on a practical distribution grid in the availability of RE.
- Performance of IDM is superior compared to DWT-based IDM and an IDM using rate of change of voltage. It detects islanding events in a small-time duration compared to voltage-supported IDM, rate of change of frequency-based IDM, and DWT-based IDM.

II. METHODOLOGY AND TEST DESCRIPTION

This section details the problem formulation and test distribution grid used for the study. The proposed algorithm for identifying islanding events and mathematical tools used to design the proposed technique has also been discussed in this section.

A. PROBLEM FORMULATION FOR ISLANDING DETECTION

The penetration of RE into the power grid has been gradually growing recently. This has resulted in feeding of power to local loads through the DG sources. In the remotely located areas, a large part of the load is being fed from the RE sources. Disconnection of such distribution network from the primary utility grid and still energized from the DG sources is known as the islanding event. There are active and passive methods to recognize islanding events. Passive IDM depends on system parameters like voltage, current, and frequency. This helps in islanding detection using data analysis. Commonly used passive IDMs are over/under voltage (OV/ UV) and frequency (OF/UF). The performance of these methods is poor and can be improved by a combination of these methods with the features extracted from the voltage and current using the signal processing techniques. It is regarded as the essential aspect of the research performed in this work.

B. TEST GRID OF IEEE-13 NODES

To simulate the islanding event, various operational and faulty events to establish execution of the IDM is tested on an IEEE-13 node test feeder simulated as a remotely located distribution grid by synchronizing the solar and wind power plants. The IEEE designs this test grid to operate at 60 Hz, 5 MVA, and feeders/loads at two different voltages of 4.16 kV and 0.48 kV. In the designed remotely located-grid network, all the loads considered are balanced in nature. This is assumed because even if there are single-phase loads, then the same will be supplied from different phases so that a balanced load will be experienced at the sending end of the feeder. Load quantum used for various nodes of the test remotely located grid is tabulated in Table 1. Details of the capacitors used in the power network are also provided in Table 1. All loads considered are constantly active and reactive powers in nature and start connected in configuration.

Further, wind power plant (WPP) of capacity 1.5 MW and solar power plant (SPP) of capacity 1 MW are integrated at the bus 680 of the test remotely located grid as detailed in Fig. 1. Hence, node 680 of the test remotely located distribution grid will be designated as PCC for grid integration of the renewable energy generators. WPP is based on the doubly-fed induction generator (DFIG) and integrated into the test grid using a transformer assigned the symbol T-WPP.

TABLE 1. Loading status of test system used for distribution grid.

Nodes of Test Distribution-grid	The load connected at various nodes of test Distribution -grid		Capacitor banks at different nodes of test Distribution - grid (kVAr)
	kW	kVAr	
634	400	290	
645	170	125	
646	230	132	
652	128	86	
671	1155	660	
675	843	462	600
692	170	151	
611	170	80	100
632-671	200	116	
680			
650			

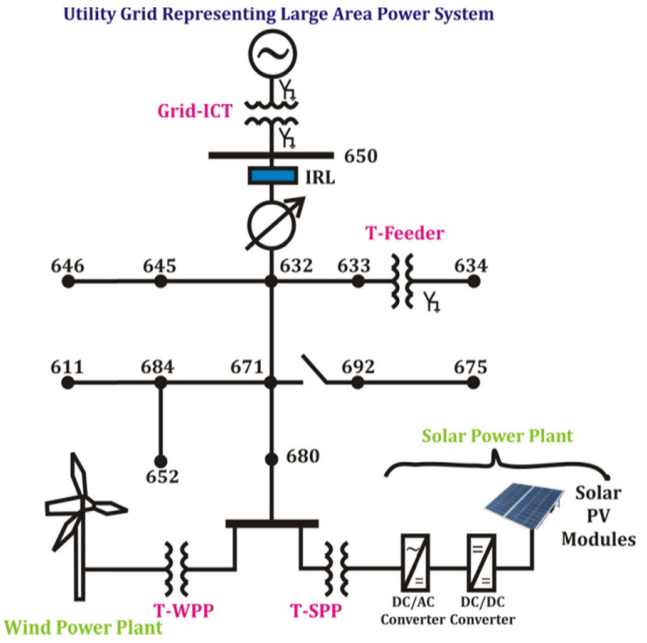

FIGURE 1. Remotely located distribution grid.

Further, a PV-based SPP of 1 MW capacity is also integrated on bus 680 of the remotely located distribution grid through a transformer assigned the symbol T-SPP. To sustain these nodes at different voltages of 4.16 kV and 0.48 kV in respective order, a transformer designated by the T-feeder is positioned between nodes 633 and 634. The test distribution grid is connected to the extensive area power system network using a transformer assigned the name Grid interconnecting transformer (Grid-ICT). The voltage ratings, MVA ratings, winding inductance, and winding resistance are compiled in Table 2. The lengths of lines used in this analysis are like those recorded in [26]–[28] for the original test system. There is a circuit breaker (CB) placed between buses 671 and 692. The wind power plant is designed using the data reported in [28].

TABLE 2. Data of transformer of test system used as a distribution grid.

Transformer	Transformer MVA rating	kV-HV winding transformer	kV-LV winding transformer	HV winding		LV winding	
				R (Ω)	X (Ω)	R (Ω)	X (Ω)
Grid-ICT	10	115	4.16	29.095	211.60	0.1142	0.8306
T-Feeder	5	4.16	0.48	0.011	3.0159	0.011	3.0159
T-WPP	5	4.16	0.575	0.3807	2.7688	0.0510	0.0042
T-SPP	5	4.16	0.260	0.001	1.1310	0.001	1.1310

Further, the solar power plant is designed using data reported in [29]. In this analysis, the voltage regulator linked among nodes 650 and 632 was not used. The islanding relay for which the algorithm is designed is placed at node 650. Hence, measurement of the voltage and current is made on this node.

C. PROPOSED ALGORITHM FOR IDENTIFICATION OF ISLANDING EVENTS

Proposed IDM used to identify islanding events is based on the application of features extracted from the current signal applying the Stockwell transform and rate of change of root mean square (RMS) current. All steps of the algorithm to identify the islanding events and differentiate these events from the operational and faulty events are illustrated in Fig. 2. A detailed description of all the steps of the algorithm for the proposed IDM is provided below:

- Record the current waveform and root mean square (RMS) values of current (IR) at the IRL node.
- Decompose the current signal using ST with a sampling frequency of 3.84 kHz and designate the output matrix as SI.
- Compute the median of the columns of the matrix SI and assign the symbol MIRF. MATLAB code used is detailed below:-

$$MIRF = median(SI)$$

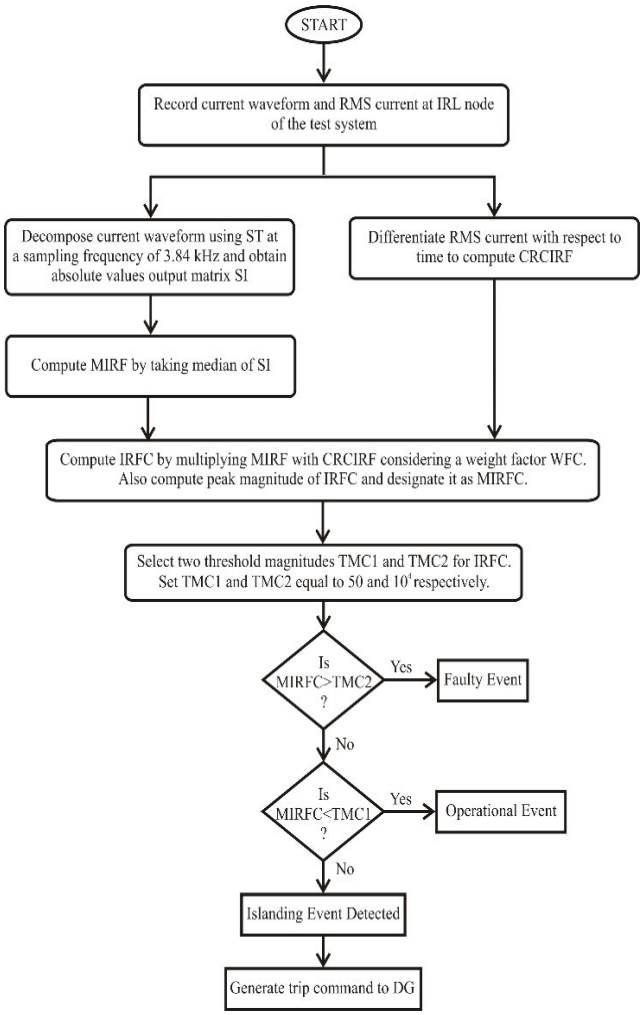

FIGURE 2. Description of proposed IDM.

- Compute the rate of change of RMS current (ROCOC) and assign the symbol CRCIRF. This is achieved using the differential operation of the Matlab, which differentiates the current signal concerning time and gives the ROCOC. Matlab code used is detailed below: -

$$CRCIRF = diff(IR)$$

- Compute the currently supported islanding recognition factor (IRFC) by multiplying the MIRF with the CRCIRF element to element, as detailed below. Here WFC is the current-based weight factor. WFC is considered equal to 10^7 for this study.

$$IRFC = MIRF \times CRCIRF \times WFC$$

Set the threshold magnitudes TMC1 and TMC2 equal to 50 and 10^4 respectively for the IRFC. If the peak magnitude of IRFC is less than TMC1, then the event is operational. For peak magnitudes of IRFC between the TMC1 and TMC2, the event is islanding. However, if the peak amplitude of IRFC is higher than the TMC2, then the event is faulty. Values of TMC1 and TMC2 are considered after testing the algorithm

on 200 data sets prepared by simulating different case studies with a wide range of parameters such as load values, capacitor values, fault incidence angle, fault impedance, RE penetration levels, and noise levels. These values are effective in the identification of islanding events in the practical distribution system. However, these values may be changed at the time of relay installation, if required depending on the RE penetration level.

Proposed IDM has been implemented in the MATLAB environment. However, for practical implementation of this IDM in distribution grids, the codes may be designed using the languages supported by the hardware of islanding relays.

D. STOCKWELL TRANSFORM (ST)

It is expressed as the expanded format of the continuous WT (CWT). This has contained the information related to the phase spectrum and magnitude. The Mother wavelet phase is essential for the extraction of information in the CWT phase for practical application. Discrete ST quickly calculates the Fast Fourier Transform (FFT) and convolution theorem using high efficiency. Results of the ST are obtained as an output complex matrix. Each row in this matrix is related to a definite frequency and substantial time for each column. Absolute value of each element of ST output are computed to obtain ST-amplitude (STA) matrix. A high time resolution is thus maintained at a high frequency and a low time resolution at a low frequency. The ST considered a multi-resolution window for which width changes inversely relative to time-changing frequency and power data. Thus, a high time resolution is maintained at high frequency, and a low time resolution is carried at a low frequency. There are several distinct ways of achieving the transformation of the ST. It introduces the relationship between the transformation of STFT, ST and the type of derivation of the transformation of ST from the ''phase correction'' of the CWT. The short Fourier Transform time of the current signal i(t) is defined by the relationship below [30].

$$\mathrm{STFT}\,(\tau, \mathrm{f}) = \int_{-\infty}^{+\infty} \mathrm{i}\,(\mathrm{t})\,\mathrm{g}(\tau - \mathrm{t})\mathrm{e}^{-\mathrm{j}2\pi \mathrm{ft}}\mathrm{dt}$$

Here τ and f are used to represent spectral localization time and Fourier frequency in respective order, and $g(t)$ is used to express a window function. ST is computed from the above relationship when g(t) is replaced by the Gaussian function described below [30].

$$g\,(t) = \frac{|f\,|}{\sqrt{2\pi}} e^{-\frac{f^2 t^2}{2}}$$

Then ST is given as

$$ST\,(\tau, f) = \int_{-\infty}^{+\infty} i\,(t)\,\frac{|f\,|}{\sqrt{2\pi}} e^{\frac{f^2(\tau - t)^2}{2}} e^{-j2\pi ft}\,dt$$

Compute absolutes values of the output matrix ST as detailed below.

$$SI = abs(ST)$$

A particular case of STFT with a Gaussian window function is the ST. If the ST window is wider in the time domain, the ST effectively provides good frequency resolution for lower frequency. Although the window is smaller, the higher frequency will provide more excellent time resolution. The output matrix ST is complex and contains information related to the frequency and amplitude of the current signal. Absolute values of the ST matrix are computed, and matrix SI is obtained, which has the exact dimensions as ST. MIRF is derived from the SI matrix.

III. ISLANDING RECOGNITION USING CURRENT BASED IRF

This section details the simulation results to recognize islanding events using the current-based islanding recognition factor (IRF). This section also details the simulation results to differentiate between operational and islanding events. The simulation results to separate the faulty events from the islanding are also described in this section. Further, it also details the findings to distinguish the islanding from the unreliable and operational events. The performance of IDM is compared at the end of the section to the algorithms mentioned in the literature.

A. HEALTHY CONDITION WITH NO DISTURBANCE

Test grid of the remotely located distribution system interfaced with the wind and solar power generators is operated for 0.2s. The current waveform and RMS value of the current (IR) are captured on the islanding relay (IRL) node and presented in Fig. 3(a) and (b), correspondingly. Signals of current are processed using Stockwell transform to compute MIRF index and described in Fig. 3(c). Moreover, the CRCIRF factor is developed by differentiating the IR and depicted in Fig. 3(d). Further, developed current based index IRFC for islanding events recognition is calculated by element-to-element multiplication of MIRF and CRCIRF with a suitable weight factor WFC. It is illustrated in Fig. 3(e).

After analysis of the current signal illustrated in Fig. 3(a), it is observed that no disturbance is related to the current signal. Further, from Fig. 2(b), it is concluded that RMS current magnitude also remains constant for the whole time duration. Additionally, it is clear from Fig. 3(c) that the magnitude of the MIRF index is constant over the entire time duration. CRCIRF index included in Fig. 3(d) indicates that there are small magnitude ripples for the whole time range, but the pattern indicates no specific disturbance linked to the current signal. The magnitude of the IRFC index included in Fig. 3(e) is constant and below the threshold TMC1. Hence, it is concluded that there is no event incident on the test system. Therefore, plots included in Fig. 3(c), (d), and (e) will be taken as reference plots to recognize the islanding events, operational events, and faulty events.

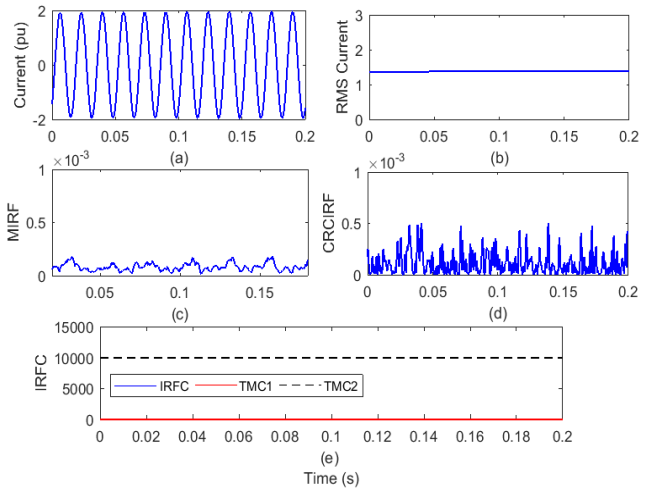

FIGURE 3. Healthy condition with no disturbance (a) current signal (b) RMS current (c) MIRF (d) CRCIRF (e) IRFC.

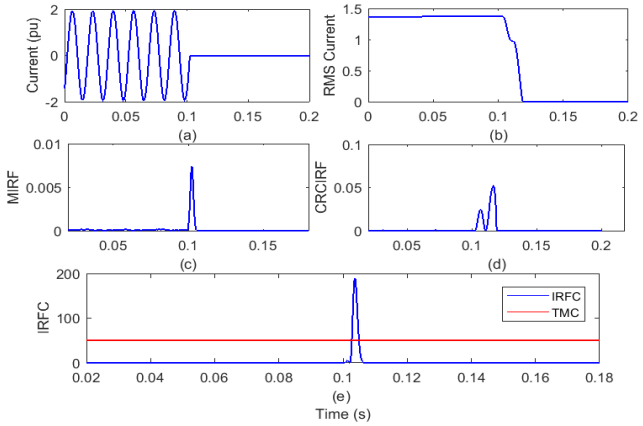

FIGURE 4. Islanding event with simultaneous availability of wind and solar power generation (a) current signal (b) RMS current (c) MIRF (d) CRCIRF (e) IRFC.

B. RECOGNITION OF ISLANDING EVENTS

The results of the recognition of Islanding events with wind generation, PV generation, and simultaneous availability of wind and solar generation are presented in this section.

1) ISLANDING WITH BOTH WIND AND SOLAR POWER GENERATION

Test grid of the remotely located distribution system interfaced with the wind and solar power generators is operated for 0.2s. Islanding is simulated at the 6th cycle by opening the circuit breaker (CB) placed near node 650 of the test grid. The current waveform and RMS value of the current (IR) is measured on the islanding relay (IRL) node and shown in Fig. 4(a) and (b) in respective order. The current signal is decomposed using Stockwell transform to compute the MIRF index described in Fig. 4(c). Further, the CRCIRF index is calculated by differentiating the IR and illustrated in Fig. 4(d). Additionally, developed current-based index IRFC for islanding recognition is calculated by element-to-element multiplication of MIRF and CRCIRF with a suitable weight factor WFC, illustrated in Fig. 4(e).

After analysing the current waveform from Fig. 4(a), it is observed that the current magnitude has reduced to zero after an incidence of the Islanding event. Further, it is also seen from Fig. 4(b) that RMS current magnitude has also decreased to zero after the incidence of the islanding event. Other minor disturbances are associated with the RMS current while reducing to zero. Additionally, it is clear from Fig. 4(c) that the amplitude of the MIRF is zero before and after the incidence of islanding. It has a peak of sharp magnitude at a moment of islanding event. CRCIRF index included in Fig. 4(d) indicates that magnitude is near zero before the incidence of the Islanding event with simultaneous wind and solar generation availability. After the incidence of the islanding, the magnitude increases and becomes high, and two high magnitude ripples are observed. The magnitude of the IRFC index included in Fig. 4(e) is zero before the incidence of islanding and becomes high at the incidence of the Islanding condition. At the moment of islanding incidence, the magnitude of the IRFC index becomes more significant than the threshold TMC1 but remains below the threshold TMC2. Hence, it is concluded that the Islanding condition with the availability of both wind and solar generation is recognized effectively and discriminated from both the faulty events and operational events.

A high-resolution plot of IRFC during the event of islanding in the presence of both wind and solar power generation is illustrated in Fig. 5. It is observed that the magnitude of IRFC crosses the TMC1 in time duration of 0.0004s first time during rising trend and again crosses the TMC1 in time duration of 0.0028s after the incidence of islanding event. Further, during this time interval, it has not crossed the TMC2. Hence, the event is recognized as an islanding event and detected in a time interval of 0.0028s, which is more minor than the time interval of 0.05cycle (0.0083s for 60 Hz frequency power supply system).

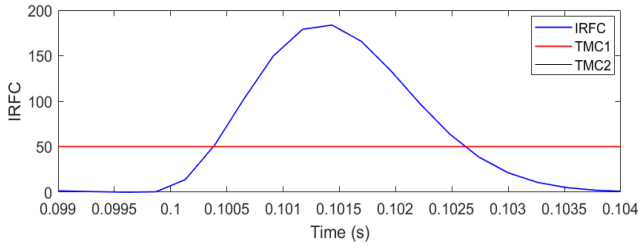

FIGURE 5. High time resolution plot of IRFC during the event of islanding in the presence of both wind and solar power generation.

2) ISLANDING IN THE AVAILABILITY OF WIND POWER PRODUCTION

The test grid of the remotely located distribution system interfaced with the wind power generators is operated for 0.2s.

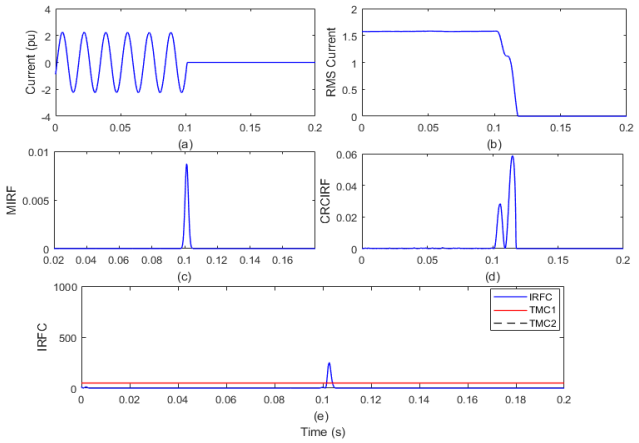

FIGURE 6. Islanding condition in the availability of wind power (a) current signal (b) RMS current (c) MIRF (d) CRCIRF (e) IRFC.

SPP remains disconnected. Islanding in the availability of WPP simulated at the 6th cycle by opening the circuit breaker (CB) placed near node 650 of the test grid. The current waveform and RMS value of the current (IR) are recorded on the islanding relay (IRL) node and shown in Fig. 6(a) and (b) correspondingly. The current signal is decomposed using ST to compute the MIRF index and described in Fig. 6(c). Further, the CRCIRF is calculated by differentiating the IR presented in Fig. 6(d). Additionally, IRFC for islanding recognition is computed by element-to-element multiplication of MIRF and CRCIRF with a suitable weight factor WFC and illustrated in Fig. 6(e).

After analysis of the current waveform from Fig. 6(a), it is observed that the current magnitude has reduced to zero after the incidence of the Islanding event. Further, it is also clear from Fig. 6(b) that RMS current magnitude has also decreased to zero after the incidence of the islanding event in the presence of WPP. Further, minor disturbances are associated with the RMS current while reducing to zero. Additionally, it is clear from Fig. 6(c) that MIRF is zero before and after the incidence of islanding in the presence of WPP. It has a sharp magnitude peak at the time of islanding in the availability of WPP. CRCIRF index included in Fig. 6(d) indicates that magnitude is near zero before the islanding incidence with wind power availability. After the incidence of the islanding event in the availability of WPP, the magnitude increases and becomes high, and two high magnitude ripples are observed. The magnitude of the IRFC index included in Fig. 6(e) is zero before the incidence of islanding in the availability of WPP. It becomes high at the moment of incidence of the islanding event in the presence of WPP. Due to the incidence of Islanding condition with the availability of WPP, the magnitude of IRFC index becomes more significant than the threshold TMC1 but remains below the threshold TMC2. Hence, it is concluded that the Islanding condition with wind power availability is recognized effectively and discriminated from the faulty events and operational events.

3) ISLANDING IN THE AVAILABILITY OF SOLAR GENERATION

The test grid of the remotely located distribution system interfaced with the solar power generators is operated for 0.2s. WPP remains disconnected. The event of islanding in the presence of SPP is simulated at the 6th cycle by opening the circuit breaker (CB) placed near node 650 of the test grid. The current waveform and RMS value of the current (IR) are measured on the islanding relay (IRL) node and illustrated in Fig. 7(a) and (b) in respective order. The current signal is decomposed using the ST and MIRF index is computed which is described in Fig. 7(c). Furthermore, the CRCIRF index is computed by differentiating the IR, illustrated in Fig. 7(d). Further, the current based index IRFC for islanding events recognition is obtained by multiplying the MIRF and CRCIRF with a suitable weight factor WFC and illustrated in Fig. 7(e).

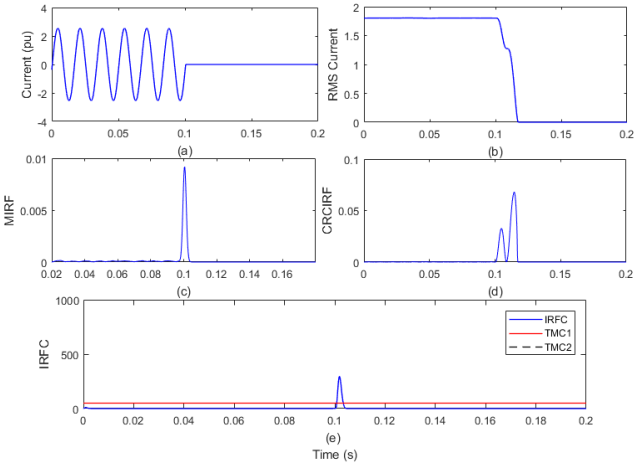

FIGURE 7. Islanding condition in the availability of solar power (a) current signal (b) RMS current (c) MIRF (d) CRCIRF (e) IRFC.

After analysing the current waveform from Fig. 7(a), it is observed that the current magnitude has reduced to zero after the incidence of the Islanding event. Further, it is also clear from Fig. 7(b) that RMS current magnitude has also decreased to zero after the incidence of the islanding event in the presence of SPP. Further, minor disturbances are associated with the RMS current while reducing to zero. Additionally, it is concluded from Fig. 7(c) that MIRF is zero before and after the incidence of islanding in the presence of SPP. It has a peak of sharp magnitude at the moment of islanding in the availability of SPP. The CRCIRF index included in Fig. 7(d) indicates that magnitude is near zero before the incidence of Islanding condition with the availability of solar power. After the incidence of islanding in the availability of SPP, the magnitude increases and becomes high, and two high magnitude ripples are observed. The magnitude of the IRFC index included in Fig. 7(e) is zero before the incidence of islanding in the availability of SPP. It becomes high at the time of incidence of the islanding in the availability of SPP. Currently, the islanding condition is incident with SPP; the magnitude of the IRFC index becomes more significant than

the threshold TMC1 but remains below the threshold TMC2. Hence, it is deduced that the islanding condition is effectively recognized in solar power generation and discriminated from both the faulty events and operational events.

C. FAULTY EVENTS

Results to recognize the faulty events such as single-phase fault, two-phase fault, two phases to ground fault, and three-phase fault involving ground using the current based IRF are discussed in this section.

1) SINGLE PHASE TO GROUND (LG) FAULT

Test grid of remotely located distribution system interfaced with WPP and SPP is operated for 0.2s. A line to ground (LG) fault is realized at node 646 of the test grid at the 6th cycle. The current waveform and RMS value of current (IR) are measured on the islanding relay location (IRL) node and shown in Fig. 8(a) and (b) in respective order. The current signal is decomposed using ST, and the MIRF index is computed, illustrated in Fig. 8(c). Further, the CRCIRF index is obtained by differentiating the IR and depicted in Fig. 8(d). Additionally, current-based index IRFC for islanding events recognition is computed by element-to-element multiplication of MIRF and CRCIRF with a suitable weight factor WFC, illustrated in Fig. 8(e).

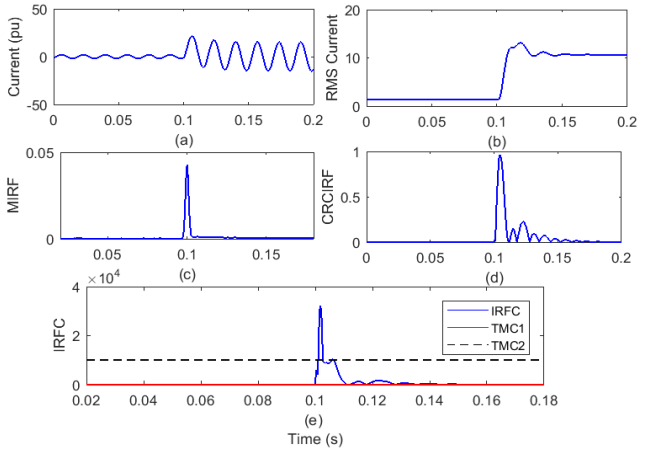

FIGURE 8. LG fault (a) current signal (b) RMS current (c) MIRF (d) CRCIRF (e) IRFC.

After analysing the current waveform from Fig. 8(a), it is observed that the current magnitude has increased after the incidence of LG fault. Further, from Fig. 8(b), RMS current magnitude has increased significantly after LG fault incidence. Additionally, low magnitude disturbances are also associated with the RMS current. Further, it is clear from Fig. 8(c) that MIRF is zero before the incidence of LG fault and becomes finite when the incidence of LG fault. After the incidence of the LG fault event, magnitude again decreases and becomes near to zero. CRCIRF index included in Fig. 8(d) indicates that magnitude is near zero before the LG fault incidence. After the incidence of the LG fault, magnitude increases and becomes high, and continuously decreasing magnitude ripples are observed and finally again becomes zero. The magnitude of the IRFC index included in Fig. 8(e) is zero before the incidence of LG fault and becomes high at the time of incidence of LG fault. Now of LG fault incidence, the magnitude of the IRFC index becomes more significant than the threshold TMC2. Hence, it is concluded that LG fault is recognized effectively and discriminated from both the Islanding event and operational events.

2) TWO-PHASE FAULTS

Test grid of the remotely located distribution system interfaced with WPP and SPP is operated for 0.2s. A two-phase (LL) fault is realized at node 646 of the test grid at the 6th cycle. The current waveform and RMS value of the current (IR) is measured on the islanding relay location (IRL) node and provided in Fig. 9(a) and (b) in respective order. The current signal is decomposed using ST to compute the MIRF index and described in Fig. 9(c). The CRCIRF index is calculated by differentiating the IR and illustrated in Fig. 9(d). Further, current-based index IRFC for islanding events recognition is obtained by multiplying the MIRF with CRCIRF with a suitable weight factor WFC, illustrated in Fig. 9(e).

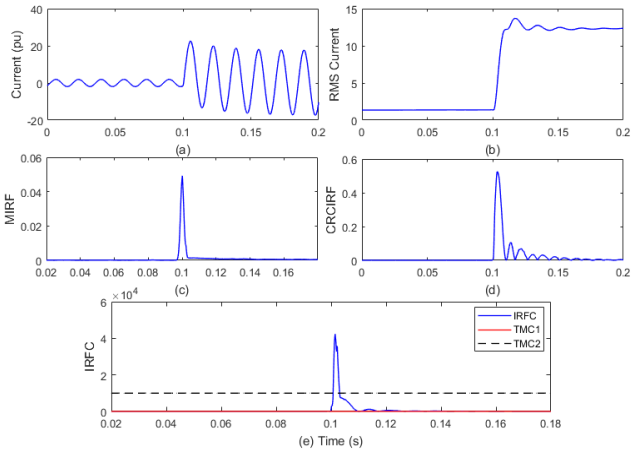

FIGURE 9. Two phase fault (a) current signal (b) RMS current (c) MIRF (d) CRCIRF (e) IRFC.

After analysis of the current waveform, Fig. 9(a) concludes that the current magnitude has increased after the incidence of LL fault. Further, Fig. 9(b) concluded that RMS current magnitude has also increased significantly after LL fault incidence. Additionally, low magnitude disturbances are also associated with the RMS current. Further, Fig. 9(c) inferred that the amplitude of the MIRF is zero before the incidence of LL fault and becomes finite at the time of incidence of LL fault. After the incidence of LL fault event, magnitude again decreases and becomes near to zero. CRCIRF index included in Fig. 9(d) indicates that magnitude is near zero before the incidence of the LL fault. After the incidence of the LL fault, magnitude increases and becomes high, and

continuously decreasing magnitude ripples are observed and finally again becomes zero. The magnitude of the IRFC index included in Fig. 9(e) is zero before the incidence of LL fault and becomes high at the time of incidence of LL fault. Now of LL fault incidence, the magnitude of the IRFC index becomes more significant than the threshold TMC2. Hence, it is concluded that LL fault is recognized effectively and discriminated from both the Islanding event and operational events.

3) TWO PHASES TO GROUND FAULT

Test grid of the remotely located distribution system interfaced with WPP and SPP is operated for a period of 0.2s. A two-phase to ground (LLG) fault is realized at bus 646 of the test grid at the 6th cycle. The current waveform and RMS value of the current (IR) is measured on the islanding relay location (IRL) node and shown in Fig. 10(a) and (b) in respective order. The current signal is decomposed using ST to compute the MIRF index described in Fig. 10(c). Further, the CRCIRF index is calculated by differentiating the IR, illustrated in Fig. 10(d). Additionally, current-based index IRFC for islanding events recognition is computed by multiplication of MIRF and CRCIRF with a suitable weight factor WFC, illustrated in Fig. 10(e).

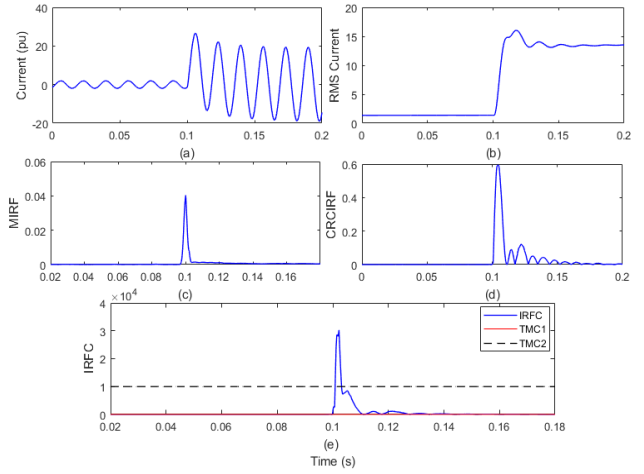

FIGURE 10. LLG fault (a) current signal (b) RMS current (c) MIRF (d) CRCIRF (e) IRFC.

After analysing the current waveform, Fig. 10(a) concludes that the current magnitude has increased after the incidence of LLG fault. Further, Fig. 10(b) presents that RMS current magnitude has also increased significantly after LLG fault incidence. Additionally, low magnitude disturbances are also associated with the RMS current. Further, Fig. 10(c) concludes that the amplitude of the MIRF is zero before the incidence of LLG fault and becomes finite at the time of incidence of LLG fault. After the incidence of LLG fault event, magnitude again decreases and becomes near to zero. CRCIRF index included in Fig. 10(d) indicates that magnitude is near zero before the LLG fault incidence. After the incidence of the LLG fault, magnitude increases and becomes high, and continuously decreasing magnitude ripples are observed and finally becomes zero. The magnitude of the IRFC index included in Fig. 10(e) is zero before the incidence of LLG fault and becomes high at the time of incidence of LLG fault. Now of LLG fault incidence, the magnitude of the IRFC index becomes more significant than the threshold TMC2. Hence, it is concluded that LLG fault is recognized effectively and discriminated from both the Islanding event and operational events.

4) THREE-PHASE FAULTS WITH GROUND

Test grid of the remotely located distribution system interfaced with WPP and SPP is operated for a period of 0.2s. A three-phase to ground (LLLG) fault is realized at node 646 of the test grid at the 6th cycle. The current waveform and RMS value of the current (IR) is measured on the islanding relay location (IRL) node and shown in Fig. 11(a) and (b) in respective sequence. The current signal is decomposed using ST to compute the MIRF index described in Fig. 11(c). The CRCIRF index is evaluated by differentiating the IR, illustrated in Fig. 11(d). Further, current-based index IRFC for islanding events recognition is computed by element-to-element multiplication of MIRF and CRCIRF with a suitable weight factor WFC, illustrated in Fig. 11(e).

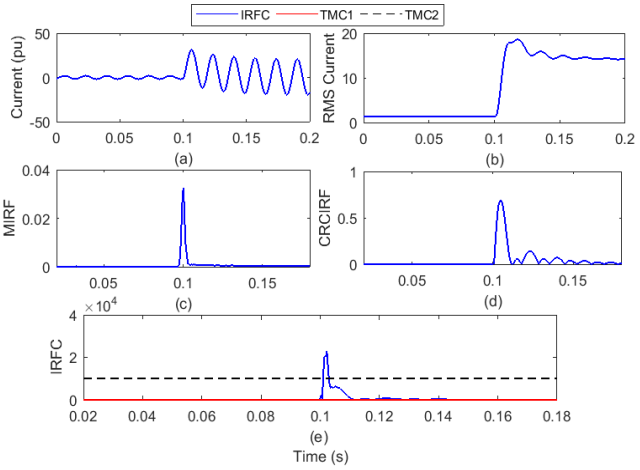

FIGURE 11. LLLG fault (a) current signal (b) RMS current (c) MIRF (d) CRCIRF (e) IRFC.

After analysing the current waveform, Fig. 11(a) concludes that the current magnitude has increased after the incidence of the LLLG fault. Further, Fig. 11(b) inferred that RMS current magnitude has also increased significantly after LLLG fault incidence. Additionally, low magnitude disturbances are also associated with the RMS current. Further, Fig. 11(c) concludes that the amplitude of the MIRF is zero before the incidence of LLLG fault and becomes finite at the time of incidence of LLLG fault. After the incidence of the LLLG fault event, magnitude again decreases and becomes near to zero. CRCIRF index included in Fig. 11(d) indicates that magnitude is near zero before the incidence of the LLLG fault. After the incidence of the LLLG fault, magnitude

increases and becomes high, and continuously decreasing magnitude ripples are observed and finally again becomes zero. The magnitude of the IRFC index included in Fig. 11(e) is zero before the incidence of LLLG fault and becomes high at the time of incidence of LLLG fault. Now of LLLG fault incidence, the magnitude of the IRFC index becomes more significant than the threshold TMC2. Hence, it is concluded that LLLG fault is recognized effectively and discriminated from both the Islanding event and operational events.

D. OPERATIONAL EVENTS

This section describes the results to recognize the operational events like outage of SPP and WPP, grid synchronization of SPP and WPP, feeder operation, switching of loads, and switching capacitors using current-based IRF.

1) OUTAGE OF WIND POWER PLANT

Test grid of the remotely located distribution system interfaced with WPP and SPP is operated for 0.2s. The WPP is disconnected from the test grid to perform an outage of WPP. On the islanding relay position (IRL) node, the current waveform and root-mean-square value of the current (IR) are recorded and shown in Fig. 12(a) and (b), in respective sequence. The current signal is processed to calculate the MIRF index using the Stockwell transform and is defined in Fig. 12(c). Also, by differentiating the IR, the CRCIRF index is computed in Fig. 12(d). The proposed current-based IRFC index for identifying islanding events is calculated with an appropriate WFC weight factor by multiplying the MIRF and CRCIRF, as shown in Fig. 12(e).

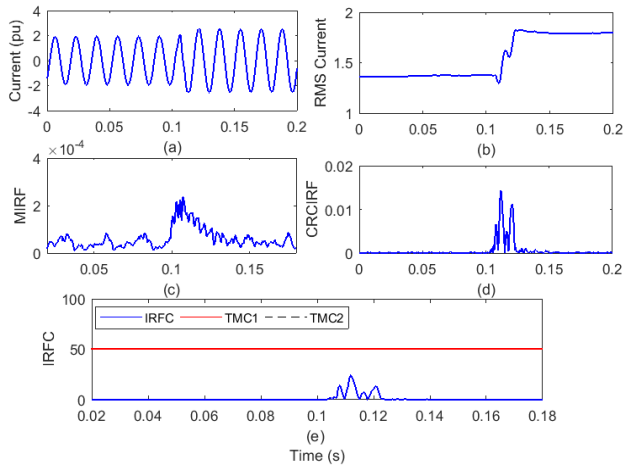

FIGURE 12. Outage of wind power plant (a) current signal (b) RMS current (c) MIRF (d) CRCIRF (e) IRFC.

After analysis of the current waveform from Fig. 12(a), it is observed that the current magnitude has increased due to the WPP outage. Further, Fig. 12(b) concludes that RMS current magnitude has increased significantly after the WPP outage. Additionally, disturbances are also associated with the RMS current. Further, Fig. 12(c) inferred that the amplitude of the MIRF had increased slightly at the time of incidence of the event of an outage of WPP. CRCIRF index included in Fig. 12(d) indicates that magnitude is near zero before the incidence of the WPP outage event. After the WPP outage event incidence, magnitude increases and becomes high for a short time duration, and finally becomes zero. The magnitude of the IRFC index included in Fig. 12(e) is zero before and after the WPP outage event. At a moment of the WPP outage event, the magnitude of the IRFC index is lower relative to threshold TMC1. Hence, it is concluded that the WPP outage event is recognized as an operational event.

2) OUTAGE OF SOLAR POWER PLANT

Test grid of the remotely located distribution system interfaced with WPP and SPP is operated for 0.2s. The SPP is disconnected from the test grid to perform an outage of the SPP. The current waveform and RMS value of the current (IR) are recorded on the islanding relay location (IRL) node and shown in Fig. 13(a) and (b), respectively. The current signal is decomposed using ST to compute the MIRF index described in Fig. 13(c). Further, the CRCIRF index is calculated by differentiating the IR illustrated in Fig. 13(d). Additionally, current-based index IRFC for recognition of islanding events is computed by multiplication of MIRF and CRCIRF with a suitable weight factor WFC, illustrated in Fig. 13(e).

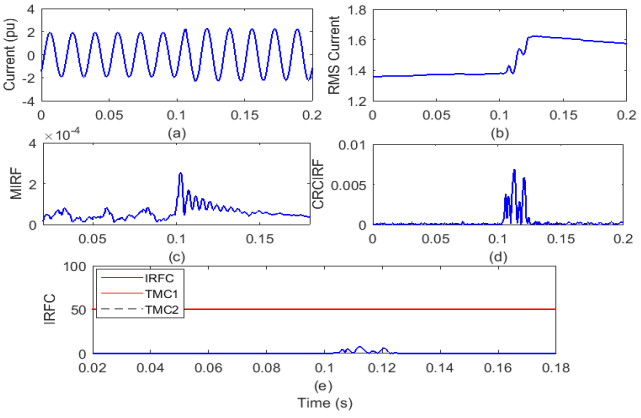

FIGURE 13. Outage of solar power plant (a) current signal (b) RMS current (c) MIRF (d) CRCIRF (e) IRFC.

After analysis of the current waveform from Fig. 13(a), it is observed that the current magnitude has increased due to the event of SPP outage. Further, it is also evaluated from Fig. 13(b) that RMS current magnitude has increased significantly after the SPP outage. Additionally, disturbances are also associated with the RMS current. Further, Fig. 13(c) concludes that the amplitude of the MIRF has increased slightly at the time of incidence of the event of an outage of SPP. CRCIRF index included in Fig. 13(d) indicates that magnitude is near zero before the incidence of the SPP outage event. After the SPP outage event incidence, magnitude increases and becomes high for a short time duration, and finally becomes zero. The magnitude of the IRFC index included in Fig. 13(e) is zero before and after the incidence

of the SPP outage event. At a moment of SPP outage event, the magnitude of the IRFC index is lower relative to threshold TMC1. Hence, it is concluded that the SPP outage event is recognized as an operational event.

3) GRID SYNCHRONIZATION OF SPP

Test grid of the remotely located distribution system interfaced with WPP is operated for 0.2s. SPP is initially kept disconnected from the test grid. The SPP is connected to the test grid at the 6^{th} cycle to perform the grid synchronization of the SPP. The current waveform and RMS value of the current (IR) is recorded on the islanding relay location (IRL) node and shown in Fig. 14(a) and (b) in respective sequence. The current signal is decomposed using ST to compute the MIRF index and described in Fig. 14(c). Further, the CRCIRF index is calculated by differentiating the IR, illustrated in Fig. 14(d). Additionally, current-based index IRFC for islanding events recognition is computed by multiplication of MIRF and CRCIRF with a suitable weight factor WFC, illustrated in Fig. 14(e).

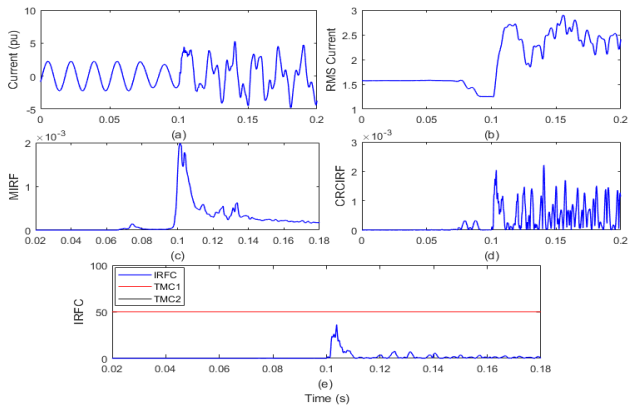

FIGURE 14. Grid synchronization of SPP (a) current signal (b) RMS current (c) MIRF (d) CRCIRF (e) IRFC.

After analysing the current waveform from Fig. 12(a), it is observed that the current magnitude is increased with sharp peak transient components due to SPP grid synchronization. Further, Fig. 12(b) concludes that transient components of low magnitude are introduced with the RMS current magnitude after SPP grid synchronization. Further, Fig. 12(c) concludes that the amplitude of the MIRF index is zero before the incidence of SPP grid synchronization and becomes finite by a small amount at the time of incidence of the event of the SPP grid synchronization. CRCIRF index included in Fig. 12(d) indicates that magnitude is near zero before the incidence of SPP grid synchronization. After the SPP grid synchronization event incidence, magnitude becomes finite and continues until the disturbances are associated with the current RMS. The magnitude of the IRFC index in Fig. 12(e) is zero before and after the SPP grid synchronization event incidence. Now of the SPP grid synchronization event, the magnitude of the IRFC index is lower relative to threshold TMC1. Hence, it is concluded that the SPP grid synchronization event is recognized as an operational event.

4) FEEDER OPERATION

Test grid of the remotely located distribution system interfaced with WPP and SPP is operated for 0.2s. Feeder comprising buses 692 and 675 is opened at 4^{th} cycle and reconnected at 8^{th} cycle to simulate the feeder tripping and closing. The current waveform and root-mean-square value of the current (IR) are measured on the islanding relay location (IRL) node and shown in Fig. 15(a) and (b) in respective sequence. The current signal is decomposed using ST to compute the MIRF index and described in Fig. 15(c). Differentiating the IR, the CRCIRF index is evaluated, illustrated in Fig. 15(d). Additionally, current-based index IRFC for islanding events recognition is computed by element-to-element multiplication of MIRF and CRCIRF with a suitable weight factor WFC illustrated in Fig. 15(e).

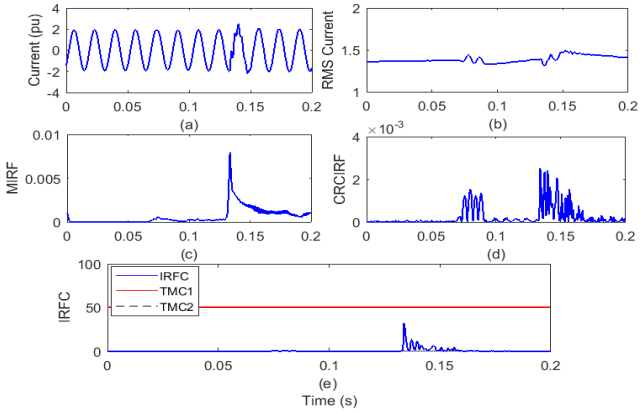

FIGURE 15. Feeder operation (a) current signal (b) RMS current (c) MIRF (d) CRCIRF (e) IRFC.

After analysis of the current waveform from Fig. 15(a), it is inferred that the current magnitude is reduced slightly at the time instant of feeder tripping and regained the value at the time of feeder re-closing. A transient of small magnitude is associated with the current now of feeder closing. It is also visible from Fig. 15(b) that at the instant of feeder tripping, the RMS current magnitude decreases and increases at the moment of feeder closure. Both the occurrence of tripping and closing the feeder has associated transient components. Also, it is compiled from Fig. 15(c) that magnitude of the MIRF index is zero before the occurrence of a feeder tripping incident. Prominent magnitude peaks at moments of tripping and closing of the feeder are observed. CRCIRF index included in Fig. 15(d) indicates that magnitude is near zero before the incidence of feeder operation. After the incidence of the feeder tripping, magnitude increases and again decreases. At the time of feeder closing, magnitude increases, and high magnitude peaks are observed till the transient components are available with the RMS current. The IRFC index magnitude used in Fig. 15(e) increases by a small

amount when tripping and closing the feeders. Magnitude, however, is lower relative to the threshold TMC1. Hence, it is concluded that the feeder operation event is recognized as an operational event.

5) CAPACITOR SWITCHING

Test grid of the remotely located distribution system interfaced with WPP and SPP is operated for 0.2s. Capacitor bank of capacity 600 kVAr connected on node 675 is disconnected at 4th cycle and reconnected at 8th cycle to simulate the capacitor switching event. The current waveform and RMS value of the current (IR) are measured on the islanding relay location (IRL) node and illustrated in Fig. 16(a) and (b) in respective order. The current signal is decomposed using ST to compute the MIRF index described in Fig. 16(c). The CRCIRF index is obtained by differentiating the IR, illustrated in Fig. 16(d). Further, current-based index IRFC for islanding events recognition is computed by element-to-element multiplication of MIRF and CRCIRF with a suitable weight factor WFC illustrated in Fig. 16(e).

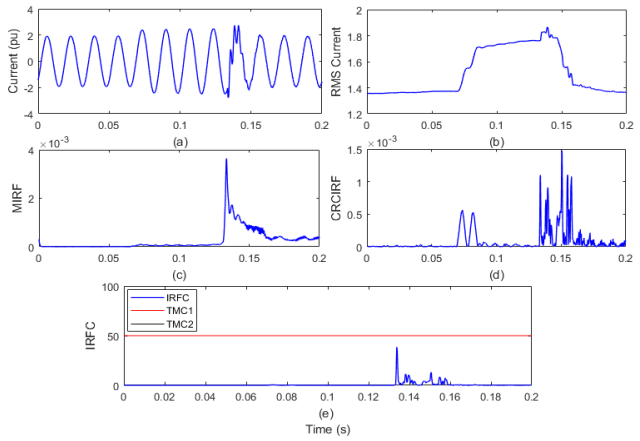

FIGURE 16. Capacitor switching (a) current signal (b) RMS current (c) MIRF (d) CRCIRF (e) IRFC.

After analysing the current waveform from Fig. 16(a), it is inferred that the current magnitude is not affected when the capacitor is switched off. However, a small magnitude transient is associated with the current when the capacitor is switched ON. Further, Figure 16 (b) shows that RMS current magnitude increases when the capacitor is switched off and decreases again when capacitors are switched on. Transient components are associated with the event of the capacitor is switched ON. Further, Fig. 16(c) concludes that the amplitude of the MIRF is zero before the incidence of capacitor operation. A small magnitude peak is observed at the time of capacitor switching off, and a high magnitude peak is kept at the capacitor switching. CRCIRF index included in Fig. 16(d) indicates that magnitude is near zero before the incidence of capacitor operation. After the incidence of the capacitor switching off, magnitude increases and again decreases. At the time of capacitor switching, the magnitude increases, and high-magnitude peaks are observed until the transient components are available with the RMS current. The magnitude of the IRFC index included in Fig. 16(e) increases by a small capacitor operation. However, magnitude is lower relative to threshold TMC1. Hence, it is concluded that capacitor operation event is recognized as an operational event.

6) LOAD SWITCHING

Test grid of the remotely located distribution system interfaced with WPP and SPP is operated for 0.2s. Load with rating 843 kW and 462 kVAr connected on node 675 is disconnected at 4th cycle and reconnected at 8th cycle to simulate the load switching event. The current waveform and RMS value of the current (IR) are recorded on the islanding relay location (IRL) node and shown in Fig. 17(a) and (b), respectively. The current signal is decomposed using ST to compute the MIRF index and described in Fig. 17(c). The CRCIRF index is calculated by differentiating the IR, illustrated in Fig. 17(d). Further, current-based index IRFC for islanding events recognition is computed by multiplication of MIRF and CRCIRF with a suitable weight factor WFC, illustrated in Fig. 17(e).

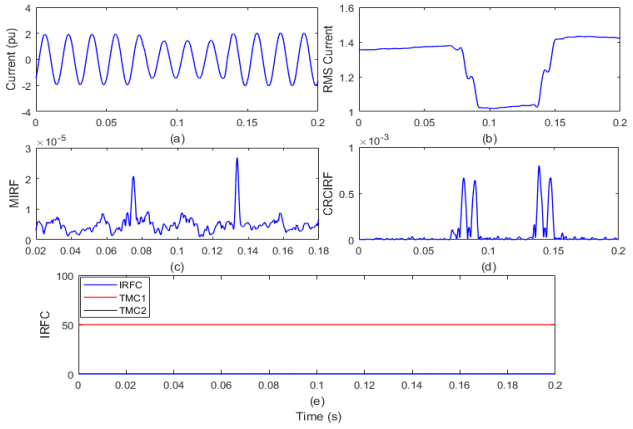

FIGURE 17. Load switching (a) current signal (b) RMS current (c) MIRF (d) CRCIRF (e) IRFC.

After the latest waveform review from Fig. 17(a), it is found that the current magnitude is reduced by switching off the load. Further, it restores the original value when the load is turned on again. Also, it is visible from Fig. 17(b) that the present magnitude of the RMS decreases after switching off the load and regains the original magnitude again after switching on the load. Transients of low magnitude components are associated with the event of the load operation. It is established from Fig. 17(c) that sharp amplitude peaks are observed at the time of load switching off and load switching on. CRCIRF index included in Fig. 17(d) indicates that magnitude is near zero before the incidence of the load operation. After the incidence of the load switching off, magnitude increases and again decreases. At the time of load switching on and off, magnitude increase, and high magnitude peaks are observed until the transient components are available with

the RMS current. The magnitude of the IRFC index included in Fig. 17(e) increases by a small amount of load operation. However, the magnitude is lower relative to the threshold TMC1. Hence, it is concluded that the load operation event is recognized as an operational event.

IV. CLASSIFICATION OF EVENTS

The classification of Islanding events, fault events, and operational events in different categories is achieved using decision rules supported by the peak magnitude of the current-based IRF. The peak magnitude of the current-based islanding recognition factor for various events is provided in Table 3.

TABLE 3. Peak magnitude of current based IRF.

S. No.	Type of Event	Peak Magnitude of IRFC
1	Healthy condition with no disturbance	0.59
2	Islanding event in the availability of both wind and solar power	185.05
3	Islanding event in the availability of wind power generation	251.30
4	Islanding event in the availability of solar power generation	291.90
5	LG fault	3.105×10^4
6	LL fault	4.235×10^4
7	LLG fault	3.029×10^4
8	LLLG fault	2.294×10^4
9	Outage of Wind power plant	24.17
10	Outage of Solar power plant	14.02
11	Synchronization of SPP	36.92
12	Feeder operation	32.08
13	Capacitor switching	38.47
14	Load switching	0.042

Classification of the events to discriminate Islanding events from the operational and faulty events is described in Fig. 18. It is observed that different events are classified one by one. If MIRFC>TMC2, then the event is faulty.

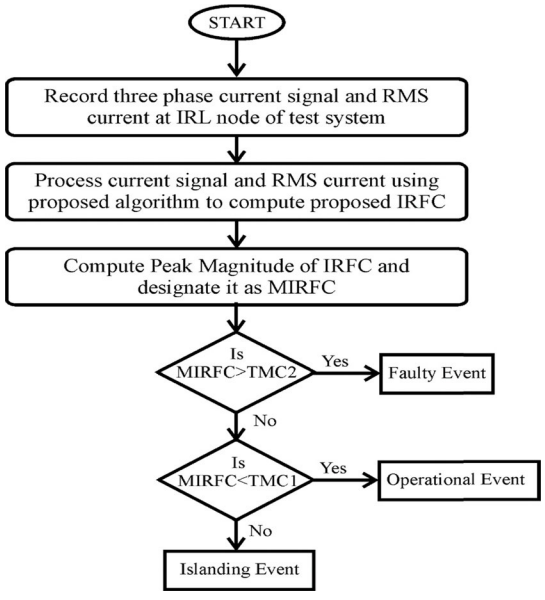

FIGURE 18. Classification of islanding and non-islanding events.

Further, if MIRFC<TMC1, then the event is operational. For the islanding events, TMC1<MIRFC<TMC2 condition is followed.

V. PERFORMANCE OF IDM ON PRACTICAL DISTRIBUTION NETWORK

The effectiveness of the proposed IDM is tested on a practical distribution system in the western parts of Rajasthan, India, where RE is integrated into significant quantum. Details of the distribution feeder used for validation in real-time are included in Table 4. This feeder is connected to a 132/33 kV Grid substation (GSS), and power is received from this GSS. Islanding event is realized by tripping this feeder from the sending end 132 kV GSS, and current is recorded. IRFC is computed using the proposed IDM and described in Fig. 19. It is observed that the peak magnitude of IRFC falls between the TMC1 and TMC2. However, the peak magnitude of the IRFC is high compared to that recorded on the test system. Hence, an islanding event incident on a practical distribution feeder has been recognized using the proposed IDM.

TABLE 4. Details of practical distribution feeder.

S. No.	Description	Capacity
1	Distribution Transformer Capacity 11/0.44 kV	18 MVA
2	Transformer Capacity 33/11 kV	24 MVA
3	Connected Load	11.032 MW
4	Connected Solar Capacity (including rooftop solar PV system)	3.15 MW
5	Connected Wind power plant capacity	2 MW

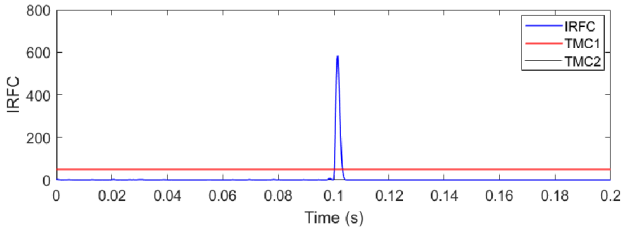

FIGURE 19. IRFC computed for an islanding event incident on a practical distribution feeder.

VI. PERFORMANCE COMPARISON OF ALGORITHM

The IDMs based on the rate of change in the voltage (ROCOV) and rate of change in frequency (ROCOF), detects an islanding event in a time of 0.25 to 0.5 cycles. In contrast, the current-based IDM investigated in this study successfully detects an islanding event in a time duration of fewer than 0.05 cycles [31]. Compared to the wavelet transform (WT) based IDM [32], the method implemented in this paper is also fast and precise. Performance of the proposed IDM and DWT-based IDM [26] is evaluated in a noisy environment, and percentage accuracy with different noise levels is illustrated in Fig. 20. It is observed that accuracy for islanding identification using DWT-based IDM [32]

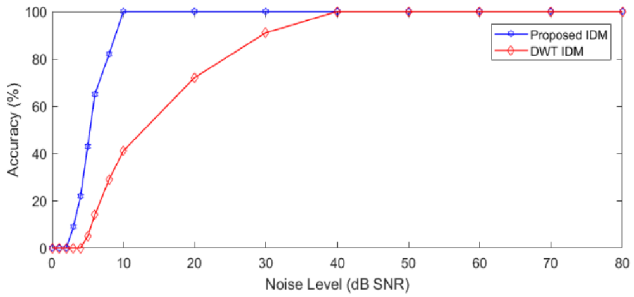

FIGURE 20. Effect of noise on the performance of IDM.

decreased for noise levels higher than 40 dB SNR. However, the proposed IDM effectively recognizes the islanding events with higher noise levels of 10 dB SNR.

VII. CONCLUSION

An IDM to identify the islanding events incident on the distribution grid with RE generation is introduced, based on current signals. The current signal recorded during an event is decomposed using ST to compute MIRF. The rate of change of RMS current is evaluated by differentiating the RMS current concerning time, and CRCIRF is calculated. Proposed current-based IRFC is calculated by multiplying the MIRF and CRCIRF with a weight factor. Threshold magnitudes TMC1 and TMC2 are set equal to 50 and 10^4, respectively, for the IRFC. Decision rules are used to discriminate the islanding events from the faulty and operational events using the peak magnitude of IRFC. If the peak magnitude of IRFC is less than TMC1, then the event is active. For peak magnitudes of IRFC between the TMC1 and TMC2, the event is islanding. However, if IRFC's peak magnitude is more significant than TMC2, then the event is faulty. It is concluded that current-based IDM successfully detects and discriminates against the defective and operational events of the Islanding events. This IDM effectively recognizes islanding events on a practical distribution feeder where DG sources are available. The performance of IDM is high even in a high noise level of 10dB SNR. Compared to the IDMs stated in the literature and based on voltage change rate (ROCOV), frequency change rate, and DWT, the proposed algorithm is found to have better performance.

REFERENCES

[1] X. Xie, C. Huang, and D. Li, "A new passive islanding detection approach considering the dynamic behavior of load in microgrid," *Int. J. Electr. Power Energy Syst.*, vol. 117, May 2020, Art. no. 105619.
[2] S. C. Paivaa, R. L. D. A. Ribeiro, D. K. Alves, F. B. Costa, and T. D. O. A. Rocha, "A wavelet-based hybrid islanding detection system applied for distributed generators interconnected to AC microgrids," *Elect. Power Energy Syst.*, vol. 121, Oct. 2020, Art. no. 106032.
[3] K. M. Tsang and W. L. Chan, "Rapid islanding detection using multi-level inverter for grid-interactive PV system," *Energy Convers. Manage.*, vol. 77, pp. 278–286, Jan. 2014.
[4] A. Taheri Kolli and N. Ghaffarzadeh, "A novel phaselet-based approach for islanding detection in inverter-based distributed generation systems," *Electr. Power Syst. Res.*, vol. 182, May 2020, Art. no. 106226.
[5] K. N. E. Ku Ahmad, J. Selvaraj, and N. A. Rahim, "A review of the islanding detection methods in grid-connected PV inverters," *Renew. Sustain. Energy Rev.*, vol. 21, pp. 756–766, May 2013.
[6] A. Samui and S. R. Samantaray, "An active islanding detection scheme for inverter-based DG with frequency dependent ZIP–exponential static load model," *Int. J. Electr. Power Energy Syst.*, vol. 78, pp. 41–50, Jun. 2016.
[7] X. Kong, X. Xu, Z. Yan, S. Chen, H. Yang, and D. Han, "Deep learning hybrid method for islanding detection in distributed generation," *Appl. Energy*, vol. 210, pp. 776–785, Jan. 2018.
[8] E. C. Pedrino, T. Yamada, T. R. Lunardi, and J. C. D. M. Vieira, "Islanding detection of distributed generation by using multi-gene genetic programming based classifier," *Appl. Soft Comput.*, vol. 74, pp. 206–215, Jan. 2019.
[9] J. R. Reddy, A. Pandian, and C. R. Reddy, "An efficient learning based RFMFA technique for islanding detection scheme in distributed generation systems," *Appl. Soft Comput.*, vol. 96, Nov. 2020, Art. no. 106638.
[10] S. Raza, T. ur Rahman, M. Saeed, and S. Jameel, "Performance analysis of power system parameters for islanding detection using mathematical morphology," *Ain Shams Eng. J.*, vol. 12, no. 1, pp. 517–527, Mar. 2021.
[11] S. R. Thomas, V. Kurupath, and U. Nair, "A passive islanding detection method based on K-means clustering and EMD of reactive power signal," *Sustain. Energy, Grids Netw.*, vol. 23, Sep. 2020, Art. no. 100377.
[12] G. Wang and S. University, "Design consideration and performance analysis of a hybrid islanding detection method combining voltage unbalance/total harmonic distortion and bilateral reactive power variation," *CPSS Trans. Power Electron. Appl.*, vol. 5, no. 1, pp. 86–100, Mar. 2020.
[13] A. G. Abd-Elkader, S. M. Saleh, and M. B. Magdi Eiteba, "A passive islanding detection strategy for multi-distributed generations," *Int. J. Electr. Power Energy Syst.*, vol. 99, pp. 146–155, Jul. 2018.
[14] M. Babakmehr, F. Harirchi, P. Dehghanian, and J. Enslin, "Artificial intelligence-based cyber-physical events classification for islanding detection in power inverters," *IEEE J. Emerg. Sel. Topics Power Electron.*, early access, Mar. 11, 2020, doi: 10.1109/JESTPE.2020.2980045.
[15] R. Bakhshi-Jafarabadi, J. Sadeh, and M. Popov, "Maximum power point tracking injection method for islanding detection of grid-connected photovoltaic systems in microgrid," *IEEE Trans. Power Del.*, vol. 36, no. 1, pp. 168–179, Feb. 2021, doi: 10.1109/TPWRD.2020.2976739.
[16] B. K. Chaitanya, A. Yadav, and M. Pazoki, "Reliable islanding detection scheme for distributed generation based on pattern-recognition," *IEEE Trans. Ind. Informat.*, vol. 17, no. 8, pp. 5230–5238, Aug. 2021, doi: 10.1109/TII.2020.3029675.
[17] M. Ahmadipour, H. Hizam, M. L. Othman, M. A. M. Radzi, and A. S. Murthy, "Islanding detection technique using slantlet transform and ridgelet probabilistic neural network in grid-connected photovoltaic system," *Appl. Energy*, vol. 231, pp. 645–659, Dec. 2018.
[18] Y. Li, N. Lu, X. Wang, and B. Jiang, "Islanding fault detection based on data-driven approach with active developed reactive power variation," *Neurocomputing*, vol. 337, pp. 97–109, Apr. 2019.
[19] B. K. Chaitanya, A. Yadav, and M. Pazoki, "An advanced signal decomposition technique for islanding detection in DG system," *IEEE Syst. J.*, early access, Aug. 31, 2020, doi: 10.1109/JSYST.2020.3017157.
[20] R. Kaushik, O. P. Mahela, P. K. Bhatt, B. Khan, A. R. Garg, H. H. Alhelou, and P. Siano, "Recognition of islanding and operational events in power system with renewable energy penetration using a stockwell transform-based method," *IEEE Syst. J.*, early access, Sep. 15, 2020, doi: 10.1109/JSYST.2020.3020919.
[21] W. Zhang, A. Maleki, F. Pourfayaz, and M. S. Shadloo, "An artificial intelligence approach to optimization of an off-grid hybrid wind/hydrogen system," *Int. J. Hydrogen Energy*, vol. 46, no. 24, pp. 12725–12738, Apr. 2021.
[22] G. Zhang, Y. Shi, A. Maleki, and M. A. Rosen, "Optimal location and size of a grid-independent solar/hydrogen system for rural areas using an efficient heuristic approach," *Renew. Energy*, vol. 156, pp. 1203–1214, Aug. 2020.
[23] A. Maleki, M. A. Nazari, and F. Pourfayaz, "Harmony search optimization for optimum sizing of hybrid solar schemes based on battery storage unit," *Energy Rep.*, vol. 6, pp. 102–111, Dec. 2020.
[24] W. Cai, X. Li, A. Maleki, F. Pourfayaz, M. A. Rosen, M. A. Nazari, and D. T. Bui, "Optimal sizing and location based on economic parameters for an off-grid application of a hybrid system with photovoltaic, battery and diesel technology," *Energy*, vol. 201, Jun. 2020, Art. no. 117480.
[25] W. Zhang, A. Maleki, A. K. Birjandi, M. A. Nazari, and O. Mohammadi, "Discrete optimization algorithm for optimal design of a solar/wind/battery hybrid energy conversion scheme," *Int. J. Low-Carbon Technol.*, early access, pp. 1–15, Sep. 2020, doi: 10.1093/ijlct/ctaa067.

[26] M. S. S. Kulshrestha, O. P. Mahela, M. K. Gupta, N. Gupta, N. Patel, T. Senjyu, M. S. S. Danish, and M. Khosravy, "A hybrid protection scheme using stockwell transform and Wigner distribution function for power system network with solar energy penetration," *Energies*, vol. 13, no. 14, p. 3519, 2020, doi: 10.3390/en13143519.

[27] A. G. Shaik and O. P. Mahela, "Power quality assessment and event detection in hybrid power system," *Electr. Power Syst. Res.*, vol. 161, pp. 26–44, Mar. 2018, doi: 10.1016/j.epsr.2018.03.026.

[28] O. P. Mahela and A. G. Shaik, "Power quality improvement in distribution network using DSTATCOM with battery energy storage system," *Int. J. Elect. Power Energy Syst.*, vol. 83, pp. 229–240, Dec. 2016, doi: 10.1016/j.ijepes.2016.04.011.

[29] O. P. Mahela and A. G. Shaik, "Power quality recognition in distribution system with solar energy penetration using S-transform and fuzzy C-means clustering," *Renew. Energy*, vol. 106, pp. 37–51, Jun. 2017, doi: 10.1016/j.renene.2016.12.098.

[30] O. P. Mahela, B. Khan, H. H. Alhelou, and P. Siano, "Power quality assessment and event detection in distribution network with wind energy penetration using stockwell transform and fuzzy clustering," *IEEE Trans. Ind. Informat.*, vol. 16, no. 11, pp. 6922–6932, Nov. 2020.

[31] T. Quoc-Tuan, "New methods of islanding detection for photovoltaic inverters," in *Proc. IEEE PES Innov. Smart Grid Technol. Conf. Eur. (ISGT-Eur.)*, Oct. 2016, pp. 9–12.

[32] R. Sharma and P. Singh, "Islanding detection and control in grid based system using wavelet transform," in *Proc. IEEE 5th Power India Conf.*, Dec. 2012, pp. 19–22.

OM PRAKASH MAHELA (Senior Member, IEEE) received the B.E. degree from the College of Technology and Engineering, Udaipur, India, in 2002, the M.Tech. degree from Jagannath University, Jaipur, India, in 2013, the Ph.D. degree from IIT Jodhpur, India, in 2018, all in electrical engineering, and the M.B.A. degree in human resource management from Indira Gandhi National Open University, New Delhi, India, in 2021. From 2002 to 2004, he was an Assistant Professor with the Rajasthan Institute of Engineering and Technology, Jaipur. From 2004 to 2014, he was a Junior Engineer with Rajasthan Rajya Vidyut Prasaran Nigam Ltd., India, and an Assistant Engineer, since February 2014. He has authored more than 170 research articles and book chapters. He performed more than 200 reviews for the prestigious journals of IEEE, Elsevier, Springer, Willey, and Taylor & Francis. His research interests include power quality, power system planning, grid integration of renewable energy sources, FACTS devices, transmission line protection, and condition monitoring. He was a recipient of the University Rank Certificate, in 2002; the Gold Medal, in 2013; the Best Research Paper Award, in 2018; and the C. V. Raman Gold Medal, in 2019. He received the certificates of outstanding contribution in the reviewing from *Computer and Electrical Engineering*, the *International Journal of Electrical Power and Energy Systems*, *Measurement*, and *Renewable and Sustainable Energy Reviews*.

YAGYA SHARMA received the B.Tech. degree in electrical engineering from the Government Engineering College Jhalawar, Rajasthan Technical University (RTU), Kota, India, in 2016, and the M.Tech. degree in power system from RTU, in 2021. Her research interests include power system operation and control, grid integration of renewable energy, and power system protection.

SHOYAB ALI received the Diploma degree in electrical engineering from the Government Polytechnic College Chittorgarh, India, in 2009, and the B.Tech. and M.Tech. degrees in electrical engineering from Rajasthan Technical University, Kota, India, in 2012 and 2015, respectively, where he is currently pursuing the Ph.D. degree. He is also working as an Assistant Professor with the Department of Electrical Engineering, Vedant College of Engineering and Technology, Bundi, India. He has authored more than 15 research articles in International journals and conferences. His research interests include improvements of power quality, FACTS controllers, and power system protection.

BASEEM KHAN (Member, IEEE) received the B.Eng. degree in electrical engineering from Rajiv Gandhi Technological University, Bhopal, India, in 2008, and the M.Tech. and D.Phil. degrees in electrical engineering from the Maulana Azad National Institute of Technology, Bhopal, in 2010 and 2014, respectively. He is currently working as a Faculty Member with Hawassa University, Ethiopia. His research interests include power system restructuring, power system planning, smart grid technologies, meta-heuristic optimization techniques, reliability analysis of renewable energy systems, power quality analysis, and renewable energy integration.

SANJEEVIKUMAR PADMANABAN (Senior Member, IEEE) received the Ph.D. degree in electrical engineering from the University of Bologna, Bologna, Italy, in 2012.

From 2012 to 2013, he was an Associate Professor with VIT University. In 2013, he joined the National Institute of Technology, India, as a Faculty Member. In 2014, he was invited as a Visiting Researcher with the Department of Electrical Engineering, Qatar University, Doha, Qatar, funded by the Qatar National Research Foundation (Government of Qatar). In 2014, he continued his research activities with the Dublin Institute of Technology, Dublin, Ireland. From 2016 to 2018, he served as an Associate Professor with the Department of Electrical and Electronics Engineering, University of Johannesburg, Johannesburg, South Africa. Since 2018, he has been a Faculty Member with the Department of Energy Technology, Aalborg University Esbjerg, Denmark. He is currently a fellow of the Institution of Engineers, India; the Institution of Electronics and Telecommunication Engineers, India; and the Institution of Engineering and Technology, U.K. He has authored over 300 scientific articles. He was a recipient of the Best Paper cum Most Excellence Research Paper Award from IET-SEISCON'13, IET-CEAT'16, IEEE-EECSI'19, and IEEE-CENCON'19, and the five best paper awards from ETAEERE'16 Sponsored Lecture Notes in electrical engineering, Springer book. He is also an Editor/Associate Editor/Editorial Board Member for refereed journals, in particular the IEEE Systems Journal, IEEE Transaction on Industry Applications, IEEE Access, *IET Power Electronics*, *IET Electronics Letters*, and *International Transactions on Electrical Energy Systems* (Wiley). He is also a Subject Editorial Board Member of *Energy Sources* (MDPI), and *Energies* Journal (MDPI). He is also a Subject Editor of the *IET Renewable Power Generation*, *IET Generation, Transmission and Distribution*, and *Facts* Journal, Canada.